Article

Journal of the Brazilian Chemical Society

https://dx.doi.org/10.21577/0103-5053.20230137

J. Braz. Chem. Soc. **2024**, *35*, 3, e-20230137, 1-11
©2024 Sociedade Brasileira de Química

The Effects of Single, Janus, and Triple Functionalization of Gold Nanoparticles on Physicochemical Properties and Cellular Uptake

Lais Helena M. da Costa,[a] *Franccesca Fornasier,*[a] *Débora A. M. de Barros,*[b] *Nilton P. da Silva,*[c] *José M. J. da Costa,*[d] *Brunno Renato F. Verçoza,*[b] *Juliany C. F. Rodrigues*[b] *and Ana Maria Percebom*[*,a]

[a]*Departamento de Química, Pontifícia Universidade Católica do Rio de Janeiro (PUC-Rio), 22451-900 Rio de Janeiro-RJ, Brazil*

[b]*Núcleo Multidisciplinar de Pesquisa em Biologia (NUMPEX-Bio), Universidade Federal do Rio de Janeiro, Campus UFRJ, Duque de Caxias Professor Geraldo Cidade, 25240-005 Duque de Caxias-RJ, Brazil*

[c]*Departamento de Engenharia Mecânica, Universidade Federal do Amazonas (UFAM), 69080-900 Manaus-AM, Brazil*

[d]*Departamento de Estatística, Universidade Federal do Amazonas (UFAM), 69080-900 Manaus-AM, Brazil*

Combining direct targeting, enhanced cellular uptake, photothermal transduction capacity, and biocompatibility in the same system is a challenge to make the application of nanoparticles in biomedicine real. This study involves the functionalization of gold nanoparticles (AuNPs) in a few steps with strategic macromolecules to provide characteristics that are key to theragnostic agents. Polyethylene glycol (PEG) is hydrophilic and can improve nanoparticle stability and circulation lifetime. Polylactic acid (PLA) is a biodegradable hydrophobic polymer important to guarantee the interaction and uptake through the cellular membranes. Folate provides specific targeting because tumors usually overexpress folate receptor proteins. Single, double, and triple functionalization of spherical and rodlike AuNPs with these ligands provided different aggregation, stability, and plasmonic properties. Triple functionalization ensured simultaneous nanoparticle stability in an aqueous medium and enhanced cellular uptake. Infrared irradiation increased the temperature of gold nanorods more than of gold nanospheres due to the longitudinal surface plasmon resonance band. The results suggest that this functionalization strategy can be used to tune the desired properties for applications of gold nanoparticles, such as imaging and photothermal therapy in biomedicine research.

Keywords: macromolecules, nanorods, metallic, coating, core-shell

Introduction

Gold nanoparticles (AuNPs) have the potential for imaging and theragnosis due to their properties associated with localized surface plasmon resonance (LSPR). However, active targeting and enhanced cellular uptake are essential to success in real applications.[1] In a previous study,[2] we prepared amphiphilic Janus AuNPs by spontaneous segregation of polymeric ligands, and they demonstrated enhanced cellular permeability. One of the hemispheres of the gold nanoparticles was functionalized with a hydrophilic polymer, polyethylene glycol (PEG), whereas the other was functionalized with a hydrophobic polymer, polystyrene (PS). While the hydrophilic side guarantees stability in aqueous media, the hydrophobic side allows interactions with the hydrophobic cellular membrane. PEG is a non-ionic, biocompatible, water-soluble polymer that effectively shields the surface charge of nanoparticles. Coating nanoparticles with PEG provides stealth properties, avoids their interaction and identification by opsonins, and increases their half-life circulation in

*e-mail: apercebom@puc-rio.br
Editor handled this article: Célia M. Ronconi (Associate)
This manuscript is part of a series of publications in the Journal of the Brazilian Chemical Society by young researchers who work in Brazil or have a solid scientific connection with our country. The JBCS welcomes these young investigators who brighten the future of chemical sciences.

This is an open-access article distributed under the terms of the Creative Commons Attribution License.

blood.[3-6] The drawback is the difficulty of interacting with cell membranes, requiring a simultaneous functionalization with a hydrophobic polymer.[5] However, PS is inadequate for biomedical applications due to its toxicity.[7] Considering the method could be extended to other polymers, poly(lactic acid) (PLA) could be an interesting substitute for PS. PLA is a hydrophobic, bio-based, and biodegradable polymer commonly used in clinical applications due to its biocompatibility and safe degradation products.[8-11] Besides, PEG and PLA have been approved by US Food and Drug Administration (FDA) for human use.[5,12-14] All the mentioned properties suggest that combining PEG and PLA to obtain Janus gold nanoparticles can efficiently and safely enhance cellular uptake.

Directing nanoparticles to the cells of interest is also essential to their application in theragnosis, requiring a functionalization that promotes active targeting. For example, folate is often used to develop tumor-targeted therapies because cancer cells overexpress folate receptors.[15,16] There are several strategies to bind folate to the surface of gold nanoparticles in the literature through covalent bonds or noncovalent interactions.[17-21] We expect that incubation of AuNPs with folate for functionalization[18] can be used previously to the Janus coating[2] to obtain a triple-functionalization. Hence, the macromolecules can give the amphiphilic character to promote cell internalization, whereas folate promotes active targeting.

The amphiphilic Janus AuNPs of our previous study[2] were spherical and presented a localized surface plasmon resonance band in the visible region (around 520-530 nm). Extending this strategy to gold nanorods could give the same properties to nanoparticles with a longitudinal plasmon band at the infrared region. When gold nanoparticles are irradiated with the same wavelength as the plasmon band, they can convert the energy into heat, quickly increasing the local temperature. When this phenomenon occurs in the infrared region, as for gold nanorods, it can be used for photothermal therapy because this radiation penetrates tissues for *in vivo* treatment.[22] The localized heating causes destructive damage to cancer cells, disrupting the cellular membrane and resulting in the ablation of tumor tissues.[23] If the nanoparticles are directed to the tumor, the heat from the photothermal therapy can irreversibly destroy cancer cells, with slight damage to normal tissues.[24]

In the present study, we propose functionalizing gold nanoparticles with thiol-terminated PEG and PLA to obtain biocompatible Janus amphiphilic nanoparticles with enhanced cellular uptake. We also evaluate using nanoparticles previously incubated with folate to obtain an active targeting system. Finally, by combining different properties in the same systems, we adapted these methods to nanorods to guarantee a multifunctional platform with potential application to photothermal therapy. The different nanoparticles obtained were characterized and used in cellular tests to verify their cytotoxicity and uptake capacity. The results allowed us to understand the role of each parameter controlled during the sample preparation. This information is essential to optimize the samples towards obtaining a multifunctional platform for diagnosing and treating cancer and other diseases.

Experimental

Materials

Tribasic sodium citrate dihydrate ($Na_3C_6H_5O_7 \cdot 2H_2O$, ≥ 99.0%), tetrachloroauric(III) acid trihydrate, ($HAuCl_4 \cdot 2H_2O$, 99%), silver nitrate ($AgNO_3$, 99.9999% trace metal basis), hexadecyltrimethylammonium bromide (CTAB, ≥ 98%), dimethyl sulfoxide (DMSO, > 99.9%), thiol-terminated poly(L-lactide) (PLA-SH, 2.5 kDa and polydispersity index (PDI) ≤ 1.2), *o*-[2-(3-mercaptopropionylamino) ethyl]-*o*'-methylpolyethylene glycol (PEG-SH, 5 kDa), and poly(sodium 4-styrenesulfonate) (NaPSS, 70 kDa) were purchased from Sigma-Aldrich (Burlington, United States). Folic acid (97%) was obtained from Oakwood Chemical (Estill, United States) and titrated with a sodium hydroxide (from Dinâmica, Belford Roxo, Brazil) solution (NaOH, 0.1 mol L^{-1}) until the equivalence point to obtain sodium folate (FOL). L-Ascorbic acid (> 99.0%) was purchased from TCI (Tokyo, Japan).

All glassware was previously washed with aqua regia so that metal contaminants would not interfere with the synthesis of the nanoparticles. Ultrapure water obtained from a system with 0.2 mm filter and resistivity above 18.2 MΩ cm was used in all the experiments.

Synthesis of gold nanospheres (AuNSs) and nanorods (AuNRs)

Gold nanospheres (AuNSs) stabilized by citrate were synthesized according to the Turkevich protocol.[25] For that, $HAuCl_4$ was reduced by sodium citrate in boiling water. Besides, gold nanorods (AuNRs) were synthesized using the seed-mediated growth method.[26] In brief, gold seeds were prepared by reducing $HAuCl_4$ with $NaBH_4$ in the presence of CTAB. In a second step, $HAuCl_4$ was reduced by ascorbic acid in the presence of CTAB, $AgNO_3$, and gold seeds to obtain nanorods with a plasmon longitudinal band at 800 nm. The obtained AuNRs were stabilized by CTAB, which is inadequate for biomedical applications and challenging for an efficient functionalization with thiol-

terminated polymers. Hence, CTAB was exchanged by citrate using a method of several centrifugations, followed by redispersion with Na-PSS or sodium citrate solutions.[27]

Functionalization of AuNSs and AuNRs

Aqueous suspensions of AuNSs and AuNRs at 5.0×10^{-5} mol L^{-1} were coated using solutions of sodium folate (FOL, 7.5×10^{-3} mol L^{-1} in water) and thiol-terminated polymers (PEG-SH and PLA-SH, 1.60×10^{-5} mol L^{-1} in DMSO) using an adaptation of our method of preparation of Janus AuNPs.[2] However, samples were prepared with only one of the ligands, or two of them (probably resulting in Janus nanoparticles), or all three. The concentration of FOL was higher than the polymer because its affinity for gold is not as intense as the affinity of thiol groups of the polymers. Due to that, when FOL was combined with the polymers for double or triple functionalization, FOL was added 15 min before the polymers. In brief, a total of 2.0 mL of the solutions of the desired ligands were added to 10.0 mL of DMSO, followed by 1.0 mL of the suspension of AuNSs or AuNRs under vigorous magnetic stirring, which was kept for 15 min. The final dispersions were left at room temperature for at least 4 h before purification. The suspensions of nanoparticles were centrifuged at 25 °C until they separated from the supernatant, which was removed and replaced with the desired solvent for removing the excess ligands. Water was the solvent of choice for the characterization of the nanoparticles and DMSO for biological analysis. This procedure was repeated twice. The period and speed rotation of the centrifugation was adapted to each system until the minimum necessary to ensure efficient separation of the supernatant. The nanoparticles were named according to their shape, AuNS or AuNR, followed by @ and the name of their ligands, FOL, PEG, PLA, or a combination of them.

Characterization of the nanoparticles

The morphology of the obtained AuNSs and AuNRs was confirmed by transmission electron microscopy (TEM), performed with a Talos F200C (Thermo Fischer Scientific, Waltham, United States) at the Brazilian Nanotechnology National Laboratory LNNano (Proposal 20210455). The dispersion of nanoparticles was drop-casted on a TEM grid (Electron Microscopy Sciences, CF-400-Cu, Hatfield, United States), and images were acquired with an acceleration voltage of 200 kV. Histograms were obtained by analyzing more than 100 AuNPs using the software ImageJ.[28]

At room temperature, the optical density spectra of dispersions of nanoparticles before and after functionalization were acquired with a UV-M51 Bel Photonics (Piracicaba, Brazil) or a Varian Cary 50 (Santa Clara, United States) spectrophotometer, using a quartz cuvette with a 1.00 cm optical path.

Distributions and mean values of the hydrodynamic diameter of the AuNPs were obtained by dynamic light scattering (DLS) experiments before and after functionalization. Measurements were performed in triplicate with an SZ-100 Nanopartica from Horiba (Kyoto, Japan), equipped with a 10 mW laser with a wavelength of 532 nm at 25.0 °C and an angle of 90°. The software HORIBA NextGen Project SZ-100 was used to treat the autocorrelation functions with Inverse Laplace Transform (ILT).

Biological analysis

Culture cell

Biological analyzes were conducted with two cell types: (*i*) LLC-MK2 kidney epithelial and (*ii*) RAW 264.7 macrophages. Cell cultures were maintained in Roswell Park Memorial Institute (RPMI) 1640 medium (Cultilab, Campinas, Brazil) supplemented with 2% sodium bicarbonate, 10% fetal bovine serum (Vitrocell, Campinas, Brazil), 100 U mL^{-1} of penicillin (Anresco, San Francisco, United States), and 10 mg mL^{-1} of streptomycin (Anresco, San Francisco, United States) at 37 °C with 5% CO_2 atmosphere in 25 or 75 cm^2 culture flasks, and in 12- or 96-well culture plates, according to each experimental analysis. The culture medium was changed three times a week, and cells were discarded when the flasks reached confluence.

Cell viability analysis

Kidney epithelial cells and macrophages were cultured in 96-well plates for cell viability analysis, as described in the "Cell culture" sub-section. For this analysis, a final concentration of 1.0×10^5 cells mL^{-1} was plated, and after 24 h of growth, 2.5 μg mL^{-1} of AuNPs with different types of functionalization was added to the respective well. Cell viability was assessed using the CellTiter 96® Aqueous MTS assay (Promega, Madison, United States) and analyzed for the 24, 48, and 72 h of treatment; each experimental group was performed in triplicate. The [3-(4,5-dimethylthiazol-2-yl)-5-(3-carboxymethoxyphenyl)-2-(4-sulfophenyl)-2*H*-tetrazolium,inner salt (MTS)/phenazine methosulfate (PMS) reaction was evaluated by optical density measured at 492 nm in a SpectraMax Paradigm microplate reader and spectrofluorometer (Molecular Devices, San Jose, USA). Statistical analysis of the data was performed with GraphPad Prism 4 software.[29]

Cellular uptake by flow cytometry

Flow cytometry was used to evaluate the cellular uptake of each nanoparticle in LLC-MK2 kidney epithelial. Cells were cultured in 12-well plates at a final concentration of 1.0×10^5 cells mL^{-1} *per* well, as described in the "Cell culture" sub-section. After 24 h of culture, cells were refrigerated at 4 °C for 30 min; after this incubation period, 2.5 μg mL^{-1} of nanoparticle was added to cultures and kept at 4 °C for another 30 min. In the sequence, cells were placed at 37 °C and kept for 30 and 60 min. At the end of each time, cells were washed three times in phosphate buffer saline (PBS) buffer supplemented with 10 mmol L^{-1} glucose pH 7.2 (PBS-glucose), removed from the culture plate with a trypsin-versene solution, washed twice in PBS-glucose and resuspended in 500 μL of the PBS-glucose buffer. Cells were evaluated by flow cytometry in an Accuri C6 cytometer (Becton Dickinson, Franklin Lakes, United States), with the reading of ten thousand events, where cell size and granularity parameters were observed.

Cellular uptake by optical microscopy

For fluorescence microscopy, 1.0×10^5 cells were cultured in 24-well plates on previously sterilized glass coverslips. After 24 h of growth, 2.5 μg mL^{-1} of nanoparticles were added to the cultures. At 1, 24, and 48 h of treatment, cells were collected, washed twice in PBS buffer pH = 7.2, and then fixed with 4% paraformaldehyde in PBS buffer for 30 min. Then, cells were washed with PBS buffer twice, and coverslips were mounted on slides using a mounting medium. Images were obtained using a Leica DMI 6000 optical fluorescence microscope (Wetzlar, Germany).

Scanning transmission electron microscopy (STEM)

Cells were cultured in 25 cm^2 bottles for scanning transmission electron microscopy as described in the "Cell culture" sub-section. After 24 h of culture, 1 μg mL^{-1} of nanoparticles was added to cultures and kept until 24 and 48 h of treatment. Control and treated cells were washed three times in PBS pH 7.2 and fixed in 2.5% glutaraldehyde in 0.1 M cacodylate buffer, pH 7.2, for 1 h. In sequence, cells were washed three times in 0.1 mol L^{-1} cacodylate buffer pH 7.2, removed from the bottom of the culture flasks with a cell scraper, and collected in an Eppendorf tube. Afterward, cells were post-fixed in a solution containing 1% osmium tetroxide, 1.25% potassium ferrocyanide, and 5 mmol L^{-1} $CaCl_2$ in 0.1 mol L^{-1} cacodylate buffer for 30 min at room temperature in the dark. Hence, cells were washed in the same buffer, dehydrated in increasing acetone concentrations (30, 50, 70, 90, and 100%), and embedded in Epon resin. Ultrathin sections were obtained in a PT-PC PowerTome ultramicrotome, stained with uranyl acetate and lead citrate, and observed in a TESCAN VEGA 3 LMU scanning electron microscope (Libušina třída, Czech Republic) operating in STEM mode at 25 kV.

Phototermal conversion

Experiments were performed to measure the temperature variation in suspensions of triple-functionalized AuNPs under the irradiation of a diode-laser (Newport, model 525B at a wavelength of 829.1 nm, Newport, United States) during 900 s, with controlled power of 439 mW and power density of 2.91 W cm^{-2}. Temperature measurements were taken with an infrared camera (Teledyne Flir, A325, Wilsonville, United States) at an acquisition rate of 1 Hz. The uncertainty associated with infrared camera calibration was 0.1 °C. The other conditions of irradiation for the photothermal experiments were defined according to the methodology described by Cruz *et al.*[30]

Results and Discussion

Functionalization with a single ligand

The shape and size of AuNSs and AuNRs were confirmed by TEM (Figure 1). After functionalization with FOL, PEG, or PLA, they exhibited different properties due to the changes in their surface properties by the coating. PEG is the most hydrophilic, and PLA is the most hydrophobic ligand. Both polymers are thiol-terminated, guaranteeing a strong binding to the gold surface. However, FOL anions bind to the gold surface mainly by the carboxylate groups, making weaker interactions than the thiol groups of the polymers and committing their hydrophilic groups.

Visual observation and dynamic light scattering results (Figure 2) indicate that PEG prevents nanoparticles from uncontrolled aggregation thanks to its hydrophilicity. The increment in the hydrodynamic diameter of AuNSs after coating with PEG can be due to the polymeric shell formed around the gold core or the formation of small aggregates. Moreover, in the case of AuNR, PEG causes a decrease in the apparent hydrodynamic diameter, probably because the AuNRs are not very stable after the exchange of CTAB by citrate, and PEG hydrophilicity can revert it. It is worth mentioning that the observation of two populations for some of the nanorods is expected due to the existence of two relaxation times related to the rotational and translational modes of the anisometric particles.[31-33] However, it means that the results do not represent the

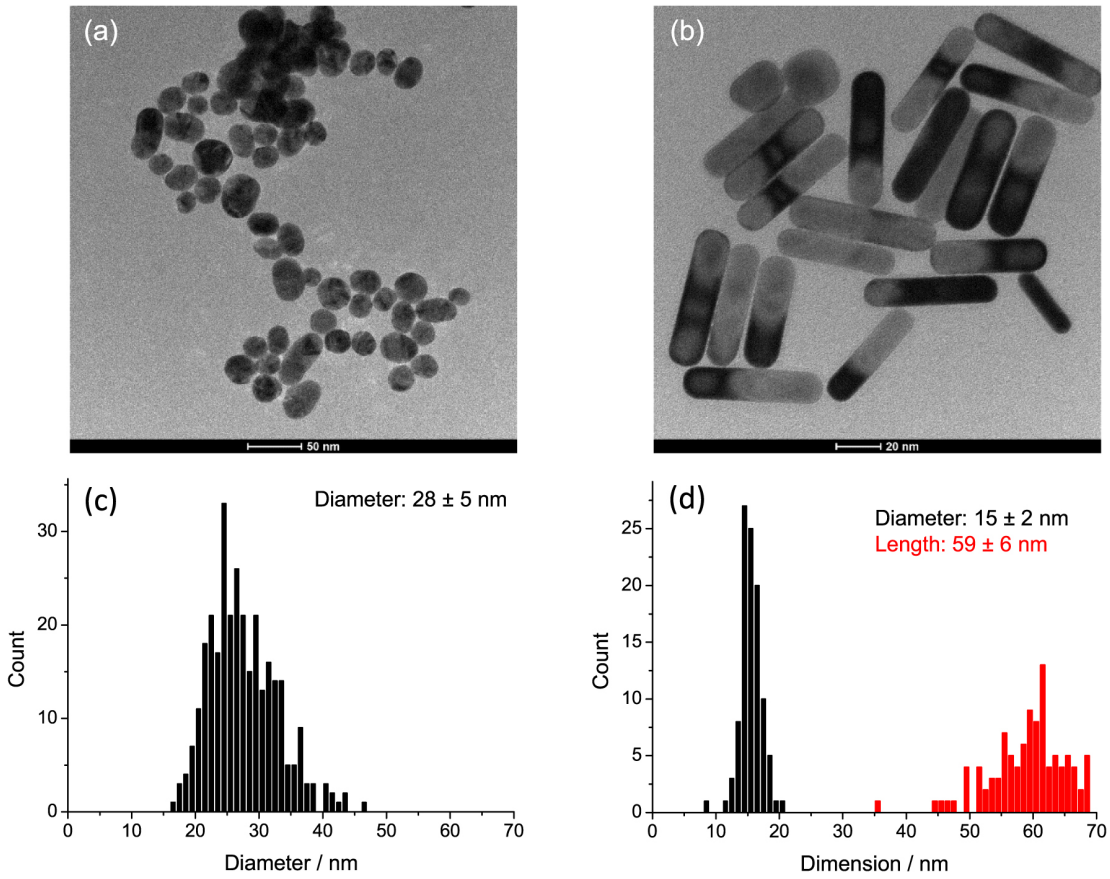

Figure 1. TEM images of (a) AuNSs and (b) AuNRs to confirm morphology and the histograms obtained by analysis of more than 100 (c) AuNSs and (d) AuNRs.

accurate real sizes, so we called it 'apparent hydrodynamic diameter', and they can be used for comparisons among the samples. FOL induces aggregation of AuNPs, causing a significant increase in hydrodynamic diameter. The aggregates formed by AuNR@FOL are so large that they are out of the size range adequate for DLS. Although it is a hydrophilic ligand, the commitment of the carboxylate groups to the gold surface does not allow them to ensure the nanoparticle's stability in the aqueous medium. Due to the hydrophobicity of PLA, the aggregates formed by AuNS@PLA and AuNR@PLA are also out of the adequate size range for DLS.

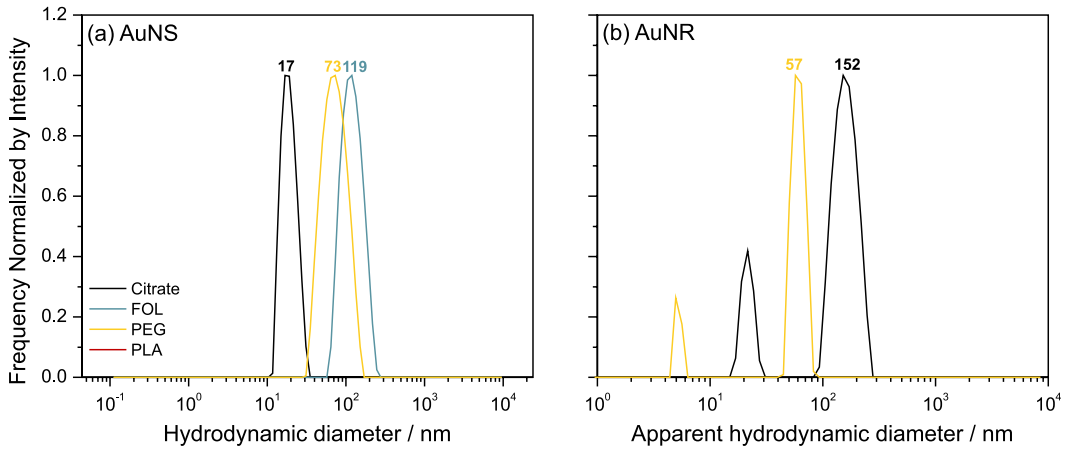

Figure 2. Dynamic light scattering results show the distribution of hydrodynamic diameters of (a) AuNSs and (b) AuNRs, with different single functionalization. The numbers refer to the mode of the distribution (in nm). Results for AuNR@FOL, AuNS@PLA, and AuNR@PLA are not visible because they were out of range. For AuNRs, the results are represented as apparent hydrodynamic diameters because they do not represent the actual sizes due to their anisometry and two relaxation modes.

The optical density spectra (Figure 3) of AuNPs confirm the observations made by DLS. When gold nanoparticles are in close proximity, their near-field can interact with each other, and the plasmon oscillations of the nanoparticles become coupled. The plasmon coupling can be observed in the spectra as a red-shift or broadening of the plasmon band.[34] The slight shift of the plasmon resonance observed after functionalization with PEG can be due to the refractive index change or a slight aggregation. FOL and PLA cause a red-shift and broadening of the plasmon resonance band, confirming the aggregation. In the case of AuNS@FOL, the result of this effect appears as a second signal around 700 nm. The characteristics of the nanoparticles after the single functionalization agree with the expected according to their intermolecular interactions. This confirmation is essential to understand the systems formed by multiple ligands.

Double and triple functionalization

According to our previous studies,[2] we expect that the functionalization of AuNSs with two antagonistic polymers forms Janus gold nanoparticles. Although we do not have results to confirm, since it is not the scope of the present study, we expect that PLA forms a hydrophobic face and PEG forms a hydrophilic face around the AuNSs. However, the adaptation of this method, combining a polymer with a smaller ligand, such as folate, is not described in the literature yet. It could also form Janus gold nanoparticles or not if the segregation tendency is insufficient. In the last case, the ligands could be homogeneously distributed or forming patches at the surface. The ligand shell morphology is not relevant for the present study, but the resultant properties are. Considering the functionalization of AuNRs, guaranteeing the Janus character is impossible, even for the combination of two polymers, because this is the first time the method has been used with gold nanorods.

When the double functionalization involves FOL as a ligand, the binding to the gold surface is weaker than when the polymers are thiol-terminated. Due to that, the nanoparticles were incubated with FOL before adding the polymers to ensure that both ligands would bind to the gold surface. DLS results (Figure 4) and optical density spectra (Figure 5) confirm that the nanoparticles differ from those with a single functionalization, indicating that both ligands are bound to the gold surface, although their proportions are unknown.

Comparing DLS results from samples with multiple functionalizations (Figure 4), AuNS@FOL-PEG form the smallest aggregates, and AuNS@FOL-PLA form the largest ones, which is expected from the hydrophilicity of PEG and hydrophobicity of PLA. AuNS@FOL-PEG and AuNS@FOL-PEG-PLA have dimensions in the same range (93 and 119 nm, respectively) and are stable for at least one year. The hydrodynamic diameter distribution (Figure 4) and the optical density spectrum of AuNP@FOL-PEG-PLA (Figure 5) differ from the results of single- and double-functionalized nanoparticles, confirming the binding of the three ligands. The same aggregation trend is observed for the multiple functionalization of AuNRs, but the aggregates of AuNR@FOL-PEG-PLA are considerably larger than AuNR@FOL-PEG. The dimensions of the aggregates formed by AuNR@PEG-PLA and AuNR@FOL-PLA are out of the adequate range for DLS. The broadening of the plasmon resonance bands of multiple functionalized AuNRs confirms that the higher the hydrophobicity of the ligands, the higher the aggregation (Figure 5).

Interestingly, the triple functionalization can form smaller aggregates and keep the system more stable in the aqueous medium than the combination of PEG and PLA.

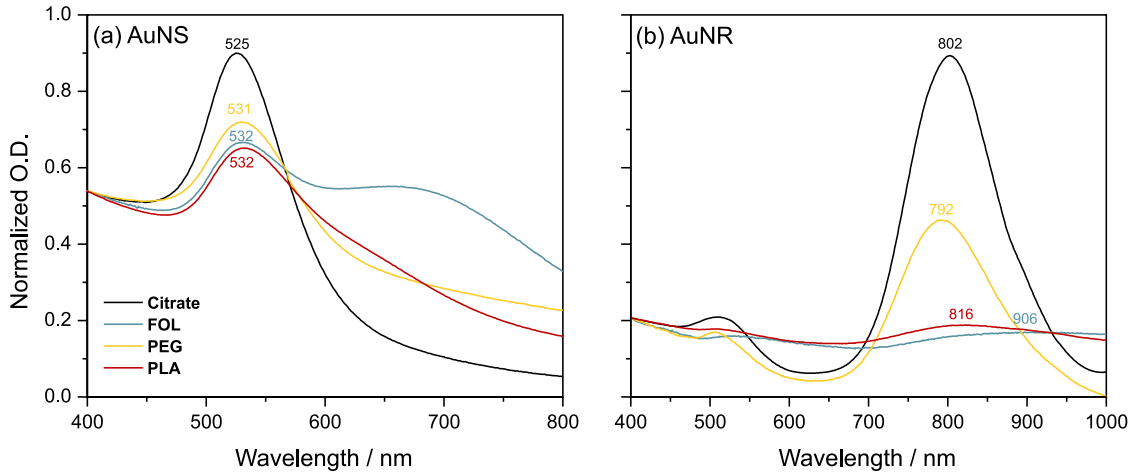

Figure 3. Normalized optical density (OD) spectra of (a) AuNSs and (b) AuNRs, with different single functionalizations. The numbers refer to the wavelength of maximum optical density for each sample.

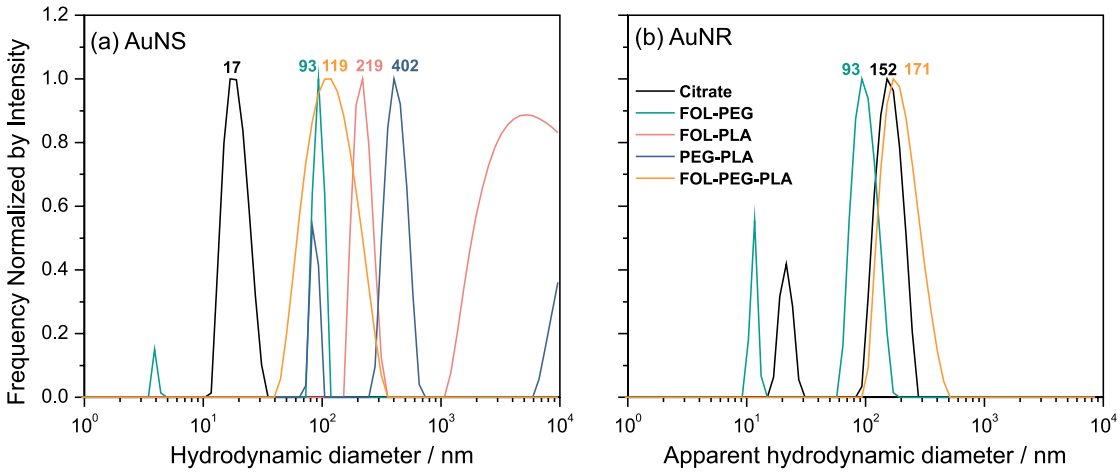

Figure 4. Dynamic light scattering results show the distribution of hydrodynamic diameters of (a) AuNSs and (b) AuNRs, with multiple functionalizations. The numbers refer to the mode of the distribution (in nm). Results for AuNR@FOL-PLA and AuNR@PEG-PLA are not visible because they were out of range. For AuNRs, the results are represented as apparent hydrodynamic diameters because they do not represent the actual sizes due to their anisometry and two relaxation modes.

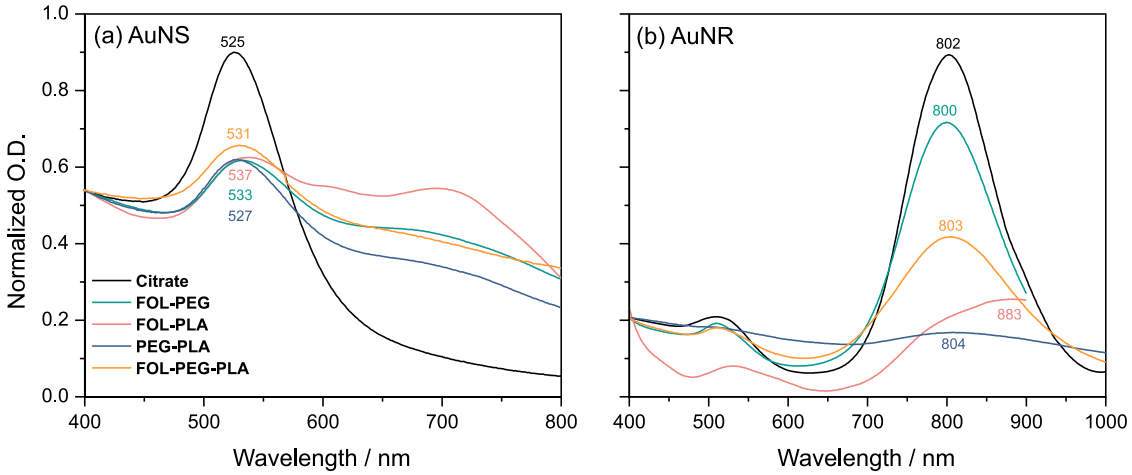

Figure 5. Normalized optical density spectra of (a) AuNSs and (b) AuNRs, with multiple functionalizations. The numbers refer to the wavelength of maximum optical density for each sample.

This characteristic is essential for practical applications. Besides, from the physicochemical properties of each ligand, one can expect that AuNP@PEG-PLA would be adequate to improve cellular uptake due to the combination of hydrophilicity and hydrophobicity but would not promote active targeting. On the other hand, the systems containing FOL as a ligand have the potential for active targeting, but the systems of AuNP@FOL-PLA form aggregates so large that they are not stable in the aqueous medium. Finally, the systems of AuNP@FOL-PEG are stable due to hydrophilicity from PEG and have FOL to promote active targeting. However, we do not know whether FOL would provide enough hydrophobicity to enhance cellular uptake. Due to that, the combination of the three ligands is expected to be the most efficient.

AuNP@FOL-PEG-PLA can have amphiphilic character due to PEG and PLA and potentially promote active targeting of cancer cells due to FOL. Although the present study does not aim to characterize the ligand shell, we expect segregation, at least for PEG and PLA, according to our previous results.[2] The Janus character is not guaranteed for AuNSs because FOL could affect the ligand distribution over the surface. However, PEG and PLA could also segregate in other morphologies, such as patches or stripes, providing amphiphilicity.

Biological analysis

Cell viability analysis

Cell viability analysis demonstrated that most systems of functionalized AuNSs were not toxic or little toxic for both cell types (LLC-MK2 epithelial cells and RAW264.7 macrophages) (Figure 6). AuNS@FOL-PLA caused a more significant cytotoxicity effect for epithelial

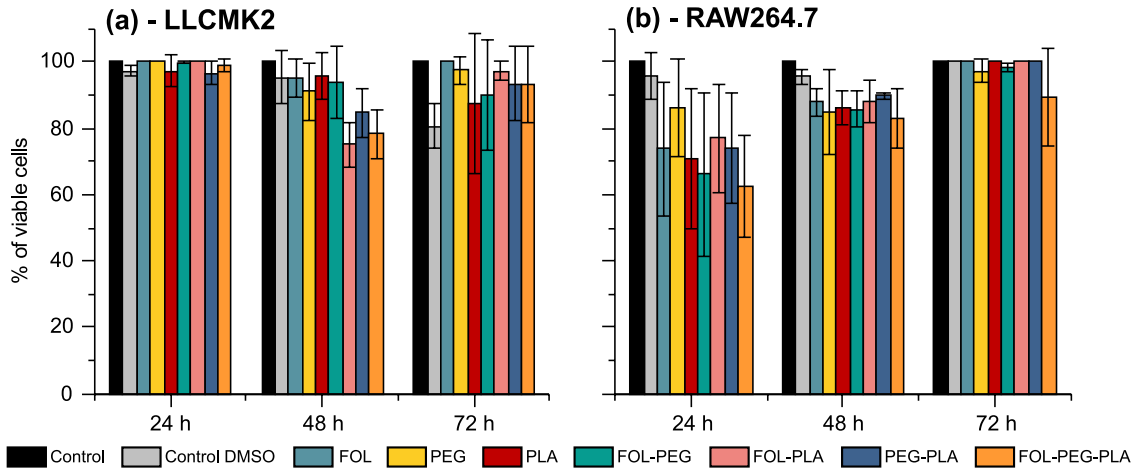

Figure 6. Evaluation of cell viability using the MTS/PMS assay. (a) LLC-MK2 kidney epithelial cells and (b) RAW 264.7 macrophages treated with 2.5 μg mL^{-1} of AuNSs with different functionalization for 24, 48, and 72 h of treatment.

cells only after 48 h of treatment and for macrophage cells after 24 h of treatment. However, the effect was reverted after 72 and 48 h, respectively, indicating the toxicity is time-dependent, according to Figure 6.

Cellular uptake

As described in the literature,[35] the flow cytometry technique can quantify the cellular uptake of AuNPs using the side scattering signal (SSC). The type of functionalization affected the cellular uptake of AuNSs by the epithelial cells, as shown in Figure 7. As expected from the preliminary results of our previous study,[2] the hydrophilicity of PEG causes the lowest internalization, which was half of the non-functionalized AuNSs and at least 5 times lower than for the other functionalized AuNSs. On the other hand, AuNS@FOL had a slightly higher uptake than AuNS@PLA, despite PLA hydrophobicity. In contrast, AuNS@FOL-PLA and AuNS@FOL-PEG-PLA (Figure 7) presented the highest uptakes at 30 and 60 min,

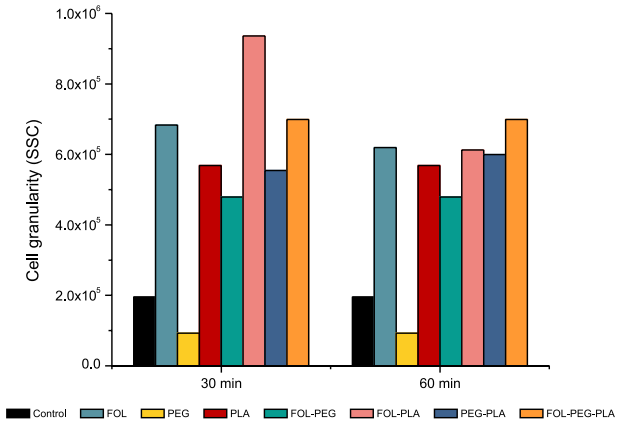

Figure 7. Evaluation of cell uptake of AuNSs with different types of functionalization by measuring cell granularity (SSC) by flow cytometry. LLC-MK2 kidney epithelial cells were treated with 2.5 μg mL^{-1} of AuNSs for 30 and 60 min.

respectively. However, AuNS@FOL, AuNS@PLA, and AuNS@FOL-PLA are inadequate for real applications due to their low stability in the aqueous medium. In addition, AuNS@PEG-PLA, which we expect to have a Janus character, presented significant uptake in both times, being a good candidate for biological applications. However, AuNS@FOL-PEG-PLA still has a higher uptake than AuNS@PEG-PLA, and could be interesting for direct targeting due to the presence of FOL, which needs to be confirmed in future studies. Therefore, we suggest AuNS@FOL-PEG-PLA as the most promising system to be further investigated in the present study.

Fluorescence optical microscopy confirmed the internalization of AuNS@FOL-PEG-PLA after 1, 24, and 48 h of treatment (Figures 8a-8f, arrows), showing an accumulation of the triple-functionalized nanoparticles as a function of time.

Scanning transmission electron microscopy (STEM)

Scanning transmission electron microscopy confirms the presence of electron-dense aggregates, corresponding to gold, randomly distributed throughout the cytosol of the LLC-MK2 epithelial cells. The aggregates inside the cells confirm the internalization of AuNS@FOL-PEG-PLA (Figures 9a-9b, arrows). Furthermore, Figure 9a shows the presence of the nanoparticles inside membrane-bounded structures (Figure 9a, arrows, and arrowhead), some connected with organelles, such as mitochondrion, and distributed throughout the cytosol (Figure 9a, arrows). Figure 9b shows the nanoparticles inside the endoplasmic reticulum of cells (arrows), sometimes associated with the membrane (thin arrows). In both micrographs, the electron-dense structures had different sizes, indicating that the nanoparticles were aggregated inside the cells.

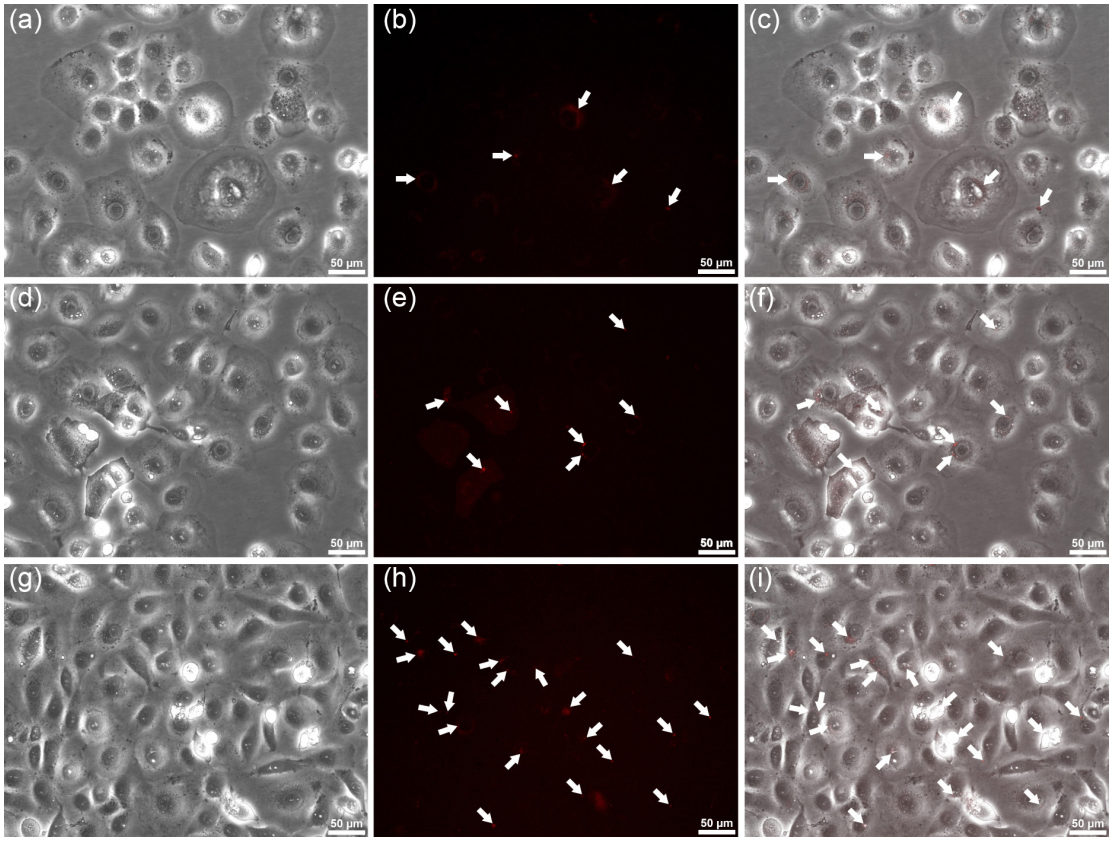

Figure 8. Optical fluorescence microscopy of LLC-MK2 kidney epithelial cells treated with 2.5 µg mL^{-1} of AuNS@FOL-PEG-PLA. (a, d, g) Phase contrast optical microscopy showing the epithelial cells with their typical morphology; (b, e, h) fluorescence of gold caused by the localized surface plasmon resonance, which is visible as punctual red markings indicated by the arrows. The fluorescence increases with treatment time, confirming the cellular uptake by the cells; (c, f, i) phase contrast images overlap with fluorescence, confirming red labeling inside some cells. (a-c) 1 h of incubation with AuNSs. (d-f) 24 h of treatment. (g-i) 48 h of treatment.

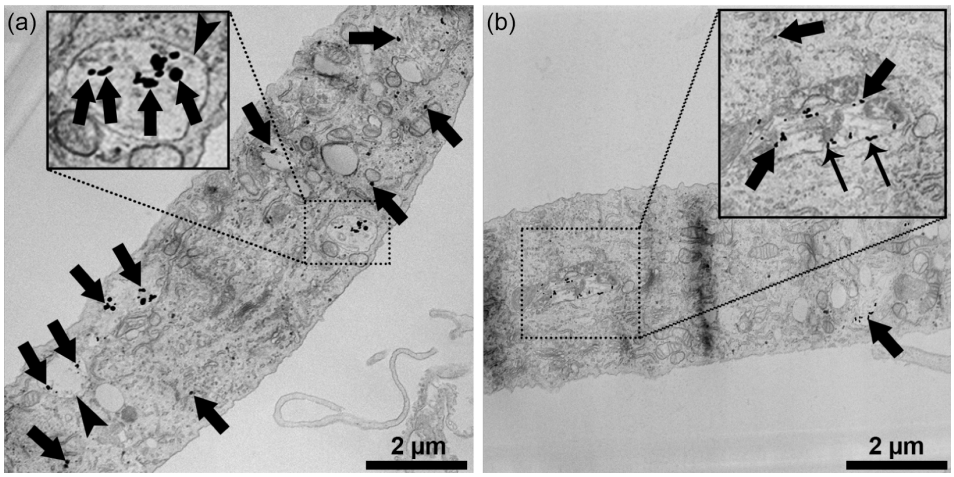

Figure 9. Scanning transmission electron microscopy (STEM) of LLC-MK2 renal epithelial cells treated with 2.5 µg mL^{-1} of AuNS@FOL-PEG-PLA. (a) This image shows the presence of NPs randomly distributed throughout the cytosol (arrows) and inside membrane-bounded structures (arrows). (b) Presence of NPs inside the endoplasmic reticulum (arrows); in high magnification, NPs are closely associated with its membrane (thin arrows).

Photothermal conversion

The efficiency of the dispersions of AuNPs as a photothermal transductor was measured by their capacity to increase temperature. Considering the interest in using infrared radiation for cancer treatment, the tests were conducted at the wavelength of 829.1 nm, and the observed variation of temperature is shown in Figure 10. The maximum variation was 2.4 °C for AuNR@FOL-PEG-PLA after 700 s. Although the plasmon band of AuNSs is in

the visible region, AuNS@FOL-PEG-PLA also induced a variation of 1.9 °C, possibly due to the broadening of the plasmon resonance band related to the coupling inside the formed aggregates. Although the samples produced heat, some parameters could still be adjusted to increase the temperature variation, such as concentration and aspect ratio of nanoparticles and laser characteristics.[36] The results confirm that nanorods have greater potential than nanospheres as transductors, indicating that AuNR@FOL-PEG-PLA would be interesting for photothermal treatment if they can be directed and selectively internalized by cancer cells.

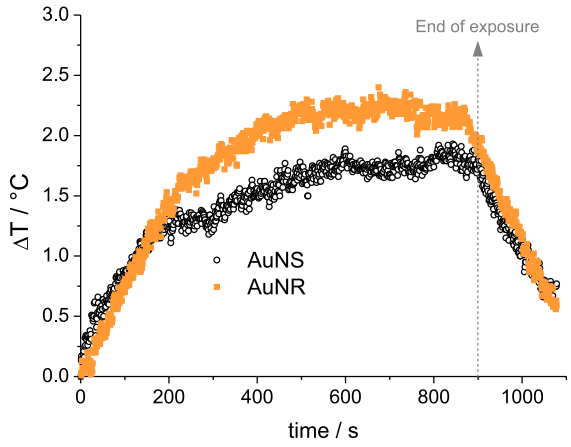

Figure 10. Variation of temperature as a function of time for AuNPs (100 μg mL^{-1}) with triple-functionalization (FOL-PEG-PLA) irradiated by a laser of 829.1 nm during 900 s.

Conclusions

The hydrophilicity and hydrophobicity of the polymers used to functionalize AuNPs were important to their final physicochemical properties, such as aggregation behavior, stability in the aqueous medium, and plasmonic effects. Although sodium folate is hydrophilic, after binding to the gold surfaces through the carboxylate group, it does not contribute to the stability of AuNPs in water. Hence, hydrophilic PEG is still necessary, but PLA and FOL can both provide the necessary hydrophobicity to promote interaction with the cellular membrane. The samples with triple functionalization have controlled aggregation and are stable in the aqueous medium. They present superior cellular uptake compared to the other systems and are efficient as photothermal transducers. AuNR@FOL-PEG-PLA can increase the temperature more than the AuNS@FOL-PEG-PLA due to the longitudinal plasmon band in the infrared region. The system can be further explored by optimization of other parameters such as the length of the polymeric chains, the proportion between the ligands, dimensions of the gold core, and concentration. All these results indicate that the system formed by triple-functionalized AuNRs has the potential for active targeting due to folate, enhanced cellular uptake due to the combination of PEG and PLA, and photothermal treatment due to the transduction efficiency of the nanorods.

Acknowledgments

We acknowledge the Nanotechnology National Laboratory (LNNano) for the use of TEM (Proposal 20210455) and the support from the staff; Central Analítica Padre Leopoldo Hainberger and Laboratório de Adsorventes para Análise Química, Proteção de Ambiente e Biomedicina (LAQAPAB) from PUC-Rio for allowing the use of the spectrophotometers, and Helcio R.B. Orlande from COPPE/UFRJ for making possible the experiments of photoconversion.

This study was financially supported by the Brazilian agencies: Fundação Carlos Chagas Filho de Amparo a Pesquisa do Estado do Rio de Janeiro (FAPERJ, Auxílio ao Pesquisador Recém-contratado E-26/211.228/2019, Programa Jovem Cientista do Nosso Estado E-26/201.422/2021, and Apoio a Projetos Temáticos, E-26/210.104/2020 for AMP; Apoio às Instituições de Ensino e Pesquisa Sediadas no RJ, E-26/010.101030/2018, and Programa Cientista do Nosso Estado E-26/201.191/2022 for JCFR) and Coordenação de Aperfeiçoamento de Pessoal de Nível Superior-Brasil (CAPES, Finance Code 001). LHMC and FF thank Conselho Nacional de Desenvolvimento Científico e Tecnológico (CNPq) for their PhD scholarships.

Author Contributions

Lais Helena M. da Costa was responsible for data curation, formal analysis, investigation, validation, writing original draft; Franccesca Fornasier for data curation, investigation, validation, writing review and editing; Débora A. Merida de Barros for data curation, investigation, validation, writing review and editing; Nilton P. da Silva for data curation, formal analysis, investigation, validation, writing review and editing; José M. J. da Costa for data curation, supervision, writing review and editing; Brunno Renato F. Verçoza for data curation, formal analysis, investigation, methodology, visualization, writing review and editing; Juliany C. F. Rodrigues for methodology, resources, supervision, writing review and editing; Ana Maria Percebom for conceptualization, funding acquisition, methodology, project administration, resources, supervision, visualization, writing review and editing.

References

1. Lee, D.-E.; Koo, H.; Sun, I.-C.; Ryu, J. H.; Kim, K.; Kwon, I. C.; *Chem. Soc. Rev.* **2012**, *41*, 2656. [Crossref]

2. Percebom, A. M.; Giner-Casares, J. J.; Claes, N.; Bals, S.; Loh, W.; Liz-Marzán, L. M.; *Chem. Commun.* **2016**, *52*, 4278. [Crossref]
3. Karakoti, A. S.; Das, S.; Thevuthasan, S.; Seal, S.; *Angew. Chem., Int. Ed.* **2011**, *50*, 1980. [Crossref]
4. Knop, K.; Hoogenboom, R.; Fischer, D.; Schubert, U. S.; *Angew. Chem., Int. Ed.* **2010**, *49*, 6288. [Crossref]
5. Zalba, S.; ten Hagen, T. L. M.; Burgui, C.; Garrido, M. J.; *J. Control. Release* **2022**, *351*, 22. [Crossref]
6. Reznickova, A.; Slavikova, N.; Kolska, Z.; Kolarova, K.; Belinova, T.; Hubalek Kalbacova, M.; Cieslar, M.; Svorcik, V.; *Colloids Surf., A* **2019**, *560*, 26. [Crossref]
7. Kik, K.; Bukowska, B.; Sicińska, P.; *Environ. Pollut.* **2020**, *262*, 114297. [Crossref]
8. da Silva, D.; Kaduri, M.; Poley, M.; Adir, O.; Krinsky, N.; Shainsky-Roitman, J.; Schroeder, A.; *Chem. Eng. J.* **2018**, *340*, 9. [Crossref]
9. Farah, S.; Anderson, D. G.; Langer, R.; *Adv. Drug Delivery Rev.* **2016**, *107*, 367. [Crossref]
10. Ramot, Y.; Haim-Zada, M.; Domb, A. J.; Nyska, A.; *Adv. Drug Delivery Rev.* **2016**, *107*, 153. [Crossref]
11. Inkinen, S.; Hakkarainen, M.; Albertsson, A.-C.; Södergård, A.; *Biomacromolecules* **2011**, *12*, 523. [Crossref]
12. Tyler, B.; Gullotti, D.; Mangraviti, A.; Utsuki, T.; Brem, H.; *Adv. Drug Delivery Rev.* **2016**, *107*, 163. [Crossref]
13. Polyethylene glycol Safety Profile, https://www.fda.gov/media/155398/download, accessed in August 2023.
14. Medical Device Material Performance Study Poly Lactic-co-Glycolic Acid [P(L/G)A] Safety Profile, https://www.fda.gov/media/155400/download, accessed in August 2023.
15. Xia, W.; Low, P. S.; *J. Med. Chem.* **2010**, *53*, 6811. [Crossref]
16. Samadian, H.; Hosseini-Nami, S.; Kamrava, S. K.; Ghaznavi, H.; Shakeri-Zadeh, A.; *J. Cancer Res. Clin. Oncol.* **2016**, *142*, 2217. [Crossref]
17. Tong, L.; Zhao, Y.; Huff, T. B.; Hansen, M. N.; Wei, A.; Cheng, J.-X.; *Adv. Mater.* **2007**, *19*, 3136. [Crossref]
18. Bhattacharya, R.; Patra, C. R.; Earl, A.; Wang, S.; Katarya, A.; Lu, L.; Kizhakkedathu, J. N.; Yaszemski, M. J.; Greipp, P. R.; Mukhopadhyay, D.; Mukherjee, P.; *Nanomed. Nanotechnol., Biol. Med.* **2007**, *3*, 224. [Crossref]
19. Asadishad, B.; Vosoughi, M.; Alamzadeh, I.; Tavakoli, A.; *J. Dispersion Sci. Technol.* **2010**, *31*, 492. [Crossref]
20. Shakeri-Zadeh, A.; Ghasemifard, M.; Ali Mansoori, G.; *Phys. E* **2010**, *42*, 1272. [Crossref]
21. Rathinaraj, P.; Lee, K.; Park, S. Y.; Kang, I. K.; *Nanoscale Res. Lett.* **2015**, *10*, 5. [Crossref]
22. Huang, X.; El-Sayed, I. H.; Qian, W.; El-Sayed, M. A.; *J. Am. Chem. Soc.* **2006**, *128*, 2115. [Crossref]
23. Dickerson, E. B.; Dreaden, E. C.; Huang, X.; El-Sayed, I. H.; Chu, H.; Pushpanketh, S.; McDonald, J. F.; El-Sayed, M. A.; *Cancer Lett.* **2008**, *269*, 57. [Crossref]
24. Ren, Y.; Yan, Y.; Qi, H.; *Adv. Colloid Interface Sci.* **2022**, *308*, 102753. [Crossref]
25. Enustun, B. V.; Turkevich, J.; *J. Am. Chem. Soc.* **1963**, *85*, 3317. [Crossref]
26. Nikoobakht, B.; El-Sayed, M. A.; *Chem. Mater.* **2003**, *15*, 1957. [Crossref]
27. Mehtala, J. G.; Zemlyanov, D. Y.; Max, J. P.; Kadasala, N.; Zhao, S.; Wei, A.; *Langmuir* **2014**, *30*, 13727. [Crossref]
28. *ImageJ*, 1.53k; Wayne Rasband, Bethesda, Maryland, United States, 2021.
29. *GraphPad Prism*, 4.0; Dotmatics, Boston, United States, 2005.
30. Cruz, C. C. R.; da Silva, N. P.; Castilho, A. V.; Favre-Nicolin, V. A.; Cesar, C. L.; Orlande, H. R. B.; dos Santos, D. S.; *Sci. Rep.* **2020**, *10*, 17561. [Crossref]
31. Rodríguez-Fernández, J.; Pérez-Juste, J.; Liz-Marzán, L. M.; Lang, P. R.; *J. Phys. Chem. C* **2007**, *111*, 5020. [Crossref]
32. Khlebtsov, B. N.; Khlebtsov, N. G.; *Colloid J.* **2011**, *73*, 118. [Crossref]
33. Berger Bioucas, F. E.; Damm, C.; Peukert, W.; Rausch, M. H.; Koller, T. M.; Giraudet, C.; Fröba, A. P.; *J. Phys. Chem. B* **2019**, *123*, 9491. [Crossref]
34. Jain, P. K.; El-Sayed, M. A.; *Chem. Phys. Lett.* **2010**, *487*, 153. [Crossref]
35. Wu, Y.; Ali, M. R. K.; Dansby, K.; El-Sayed, M. A.; *Anal. Chem.* **2019**, *91*, 14261. [Crossref]
36. Li, J.; Wang, S.; Fontana, F.; Tapeinos, C.; Shahbazi, M.-A.; Han, H.; Santos, H. A.; *Bioact. Mater.* **2023**, *23*, 471. [Crossref]

Submitted: May 30, 2023
Published online: August 14, 2023